PAPER AAS 01-411

Mars Global Surveyor Orbit Determination Uncertainties Using High Resolution Mars Gravity Models

Eric Carranza, Dah-Ning Yuan, Alex Konopliv
Jet Propulsion Laboratory, California Institute of Technology, Pasadena, CA

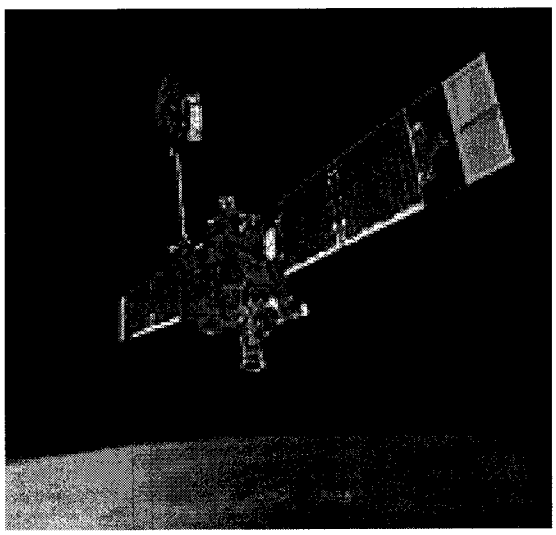

AAS/AIAA Astrodynamics Specialists Conference
Quebec City, Quebec, Canada July 30 - August 2, 2001
AAS Publications Office, P.O. Box 28130, San Diego, CA 92198

AAS 01-411

Mars Global Surveyor Orbit Determination Uncertainties Using High Resolution Mars Gravity Models

Eric Carranza*, Dah-Ning Yuan*, Alex Konopliv*

The orbit determination work on the Mars Global Surveyor presented in this paper was performed at the Jet Propulsion Laboratory and was conducted for the purpose of refining the Mars gravity field, as part of the radio science investigation. The orbit determination was performed using X-band one-way, two-way, three-way Doppler data, and two-way range data collected primarily from the Deep Space Network 34 m HEF tracking stations. A description of the mission and its trajectory will be provided, followed by a discussion of the orbit determination estimation procedure and models. Accuracies will be examined in terms of orbit-to-orbit solution differences and are determined for the latest 75th degree gravity model for the nominal mission.

INTRODUCTION

On November 7, 1996, the Mars Global Surveyor (MGS) spacecraft was launched from Cape Canaveral, Florida aboard a Delta II vehicle. MGS was part of NASA's Mars Surveyor Program, which was developed as an aggressive, low-cost program to explore Mars from 1997 to 2006. It was the first of two successful missions launched to Mars that year by NASA. The science objectives for this mission were to study the Mars atmosphere, geology, surface-atmosphere interaction, determine a global composition map and a topographic map of the surface, and improve knowledge of the magnetic and gravity fields for one Martian year. MGS arrived at Mars on September 11, 1997 and was placed into a highly elliptical near polar orbit with a periapsis altitude of 260 km, an apoapsis altitude of 54,000 km, and an orbit period of 45 hours. On September 17, 1997, aerobraking was implemented on MGS in which the spacecraft was repeatedly passed through the upper atmosphere of Mars to slow itself down by means of atmospheric drag, resulting in a lower apoapsis. The original mission plan was to use this aerobraking scheme to lower the apoapsis altitude from 54,000 km to 450 km over a four month period. However, on October 11, 1997 the scheme was suspended after one of the two solar panels on the spacecraft was bent backward because the air pressure on MGS was too high.

---

* Members of Technical Staff, Navigations and Mission Planning Section, Jet Propulsion Laboratory, California Institute of Technology, Pasadena, CA, 91109.

Aerobraking resumed on November 7, 1997, after flight team members determined that aerobraking could be safely performed on MGS at a less aggressive pace. The new plan involved two gentle aerobraking phases, two science phasing orbit phases, and a quite period during the solar conjunction period (See Table 1). The aerobraking phases were referred to as AB-1 and AB-2, which occurred from early Nov '97 to the end of Mar '98 and from the end of Sep '98 to the early part of Feb '99, respectively. The science phases were referred to as SPO-1 and SPO-2, which occurred from late Mar '98 to the end of Apr '98 and from early Jun '98 to the end of Sep '98, respectively. The quite period occurred from the end of Apr '98 to the beginning of Jun '98. The suspension of the aerobraking was necessary for two reasons: the first was to avoid aerobraking operations with degraded tracking data due to solar conjunction; the second was to allow the orbit of MGS to drift into the desired 2 PM Sun-synchronous orbit orientation. To maximize the efficiency of the mission, MGS collected as much science data as possible during this period of suspension. From early Feb. '99 to late March '99, MGS was in the gravity calibration orbit phase (GCO). On March 29, 1999, MGS began its mapping phase of the mission from a near polar circular orbit with an orbit period of about 2 hours and a periapsis altitude of 380 km (see Fig. 1). The nominal mission ended on January 31, 2001.

The orbit determination of MGS presented in this paper was performed at JPL and was conducted as part of the radio science investigation of the Mars gravity field. This paper describes the JPL effort in support of this investigation; the support includes high precision orbit determination, gravity model validation, and data editing. Two spherical harmonic Mars gravity models (MGS75B model[1] and the MGS75D model[2]) were compared to each other by studying their orbit determination errors. The data used in the creation of the MGS75B model were from the Mariner 9 mission, the Viking I and II missions, and data from the MGS mission up to the end of the GCO phase. The data used in the creation of the MGS75D model were the same data used for MGS75B, with different/additional data sets from the MGS mission; in particular, data from SPO-1, SPO-2, GCO, Map-1, Map-2, and Map-3.

SPACECRAFT DESCRIPTION

The Mars Global Surveyor spacecraft was built by Lockheed Martin Astronautics of Denver, CO and was managed by JPL. It was shaped like a rectangular box, with a 1.5 m square base and a height of 3 m. The spacecraft had four solar array panels, attached in pairs to opposite sides of the spacecraft bus like wings (See Fig. 2), and drag flaps at the tips. MGS weighed approximately 1060 kg at launch; the bus weighed about 600 kg, the science payload weighed about 70 kg, and the fuel weighed about 390 kg. The spacecraft carried six science instruments: the Mars Orbiter Camera (MOC), the Thermal Emission Spectrometer (TES), the Mars Orbiter Laser Altimeter (MOLA), the Magnetometer/Electron Reflectometer (MAG/ER), the Mars Relay system (MR), and the Ultra-stable Oscillator (USO). There were multiple science objectives for each instrument; a brief single objective statement follows. The MOC was used to obtain

high-resolution pictures of the Martian surface and atmosphere. The TES was used to map the composition of Mars minerals, rocks, and ices, and determine atmospheric temperature, pressure, water vapor, and ozone profiles. The MOLA was used to determine a global topographic grid of Mars. The MAG/ER was used to establish the nature of the Mars Magnetic Field. The MR tested the ability to establish a link with Earth tracking stations using UHF radio for the purpose of potentially relaying data from future Mars mission landers. The USO was used by Radio Science to develop a global, high-resolution Mars gravity field model.

MGS had two transmitting Low-Gain Antennas and one High-Gain Antenna. It was during the nominal mapping mission that MGS used the High-Gain Antenna (HGA) in the deployed configuration to communicate with the Deep Space Network (DSN). Prior to the start of the mapping phase, the HGA was used in the stewed configuration and did not articulate. The High-Gain Antenna was 1.5 m in diameter and sat on a boom 2 m long; it had a maximum up-link data rate capability of 500 bps. The instrument and engineering data were down-linked to the DSN tracking stations at a maximum data rate of 85.3 kbps. The tracking data used in this work were X-band up-link and down-link; the up-link was acquired at 7.9 GHz and the down-link was 8.4 GHz for two-way and three-way data.

ORBIT DETERMINATION MODELING

The orbit determination of MGS was performed using X-band one-way, two-way, three-way Doppler and two-way range data. The data was collected primarily by the DSN 34m diameter HEF tracking stations; mostly, the data was collected during the ascending portion of the orbit and smaller amounts during the descending portion of the orbit when Mars did not occult the spacecraft. The Doppler data was compressed and used in the orbit determination process as 10 second sample rate data; range data was compressed and used as 2 minute sample rate data. During the nominal mission, the one-way Doppler data was weighted with a sigma of 1mm/sec, the two- and three-way Doppler data were weighted with a sigma of 0.1 mm/sec, and the range data was weighted with a sigma of 2 meters. Invalid data were removed and corrections to the data included biases, per track station range calibration errors, and station dependent processing errors. High fidelity troposphere and ionosphere calibrations were utilized. The spacecraft attitude, high-gain antenna orientation, and Angular Momentum Dump (AMD) information were also used in the orbit determination of MGS. The orientation of the solar array panels was modeled as face on to the Sun. The spacecraft was modeled as a bus with two plates. The *a priori* sigma values for each of the spacecraft's position components were 1,000 km and were 1 km/sec for each of the velocity components.

The software used to process the tracking data was JPL's Orbit Determination Program (ODP)[3]. The ODP solves for spacecraft position, velocity, and other requested parameters using a square root information (SRIF) weighted least squares filter[4,5]. The orbit fits were done on an HPJ5600 workstation. The dynamic models used in

determining the MGS orbits were the newtonian point-mass model, the relativity model, the oblateness and solid tide models, the small forces model, the atmospheric drag model, and the solar and Mars radiation pressure models. The newtonian point-mass model computed the gravitational acceleration of the spacecraft due to the nine planets, the Sun, the Moon, Phobos, and Deimos by treating the bodies as point-masses. The relativity model computed the relativistic perturbative acceleration caused by the Sun and Jupiter on Mars. The oblateness and solid tide models computed the acceleration of the spacecraft due to Mars' oblateness and the tidal acceleration effect of the Martian solid tides caused by the Sun, respectively. The small forces model gave the spacecraft instantaneous position and velocity increments at the times of AMD events. The atmospheric drag model computed the deceleration of MGS caused by the Mars atmosphere. The solar and Martian radiation pressure models computed the acceleration of the spacecraft due to solar radiation and radiation from the Mars surface.

Other models that were used in the ODP include the solid Earth tide correction model, the continental plate motion and ocean loading models, the precession and nutation models, and the relativistic light time correction model. The precession and nutation models used the JPL Earth Orientation Parameters[6]. The Earth-fixed coordinate system used in the ODP was consistent with the International Earth Rotation Service (IERS) terrestrial reference frame labeled ITRF93[7]. The locations of the DSN stations were consistent with the ITRF93 reference frame[8]. The Mars-fixed coordinate system was consistent with the IAU 1991 orientation of Mars[9]. The ephemerides of the Sun, the Moon, and the planets were defined by the JPL DE405 planetary ephemeris[10,11]. The ephemerides of Phobos and Deimos were defined by the JPL MARS033 satellite ephemeris[12]. The inertial coordinate system used for orbit integration was Mars centered, Earth mean equator and vernal equinox system at J2000.

ESTIMATED PARAMETERS

The orbit determination process solved for the following set of estimated parameters: spacecraft position and velocity at epoch, solar radiation pressure coefficients per data arc, drag coefficients per orbit, small forces at AMD events, Doppler biases, and range biases. The Doppler biases included pass dependent biases for one-way and three-way data and a single two-way bias for a given solution. The range biases were pass dependent biases, as well. The method of estimation may be reviewed in Gravity Field of Mars: A 75th Degree and Order Model[2] by *Yuan et al.*.

ORBIT OVERLAP COMPARISONS

Each set of solutions was determined by processing a two-day data arc or a four-day data arc. The data arcs were time continuous, thus, the end time of an arc was the begin time of the next arc. The orbit determination errors were accessed by calculating the orbit overlap differences between adjacent arcs, or root-mean-square (RMS) position

differences. Hence, each arc was extended by six hours, equivalent to three orbits, and reprocessed to conduct the comparisons. The differences were relative errors between arcs and were presented in the RTN coordinate frame; *i.e.,* in the radial, transverse, and normal directions. As an aside, no predicted orbits were generated and compared to actual orbits due to the number of AMD events that occur on any given day; on the average, there are four AMD events per day. This type of comparison is another method of accessing the gravity models.

The best quality of tracking data acquired for MGS was during the GCO phase. This was so was because during the GCO phase, the High-Gain Antenna was in the stewed configuration and did not articulate. When the HGA was deployed, the position of the phase center in the spacecraft coordinate system[13] was calculated with azimuth and elevation gimbals angles retrieved from telemetry data by the NAIF mission operation team[14]. Telemetry outages introduced errors into the orbit determination solutions, which were not present when the HGA was stewed. The GCO quality of data yielded small errors. Figures 3, 4, and 5 show the radial, transverse, and normal orbit overlap errors respectively for the GCO phase of the mission. Each plot shows the overlap errors for both gravity fields, MGS75B[1] and MGS75D[2]. Results indicated an improvement in all three components. The radial overlap errors for the MGS75D model were typically less than 0.2 m; the transverse errors were typically less than 5 m; and the normal errors were typically less than 30 m.

For the nominal mapping mission, phases Map-2 and Map-3 were selected as the periods in which the overlap errors were computed. The results indicated a more significant improvement in the transverse and normal errors. The improvement was a consequence of a globally distributed data set collected during the mapping phase, the use of optimal weighting and constrained least squares solution techniques[15], and improved force and measurement models in the orbit determination process[2]. The overlap errors for MGS75D were typically less than 6 m in the radial component, less than 100 m in the transverse component, and less than 25 m in the normal component (See Fig. 6, 7, & 8). However, when the error values for the GCO phase were compared to those for the Map phases, it was noted that the GCO phase had smaller errors. This supported the idea that the best quality of data was acquired during the GCO phase. Figures 9 and 10 show sample residual plots for both two-way Doppler data and two-way range data from an MGS75D arc during the Map phase. In Fig. 11, the two-way Doppler RMS history is shown for Map-2 and Map-3. The average data arc had a two-way Doppler RMS value of 0.08655 mm/sec.

CONCLUSIONS

Two spherical harmonic Mars gravity models (MGS75B and MGS75D) of degree and order 75 were developed using historical data from the Mariner 9, Viking I, and Viking II missions, as well as data from the MGS mission. Validation and comparison of the MGS75D model with the MGS75B model was performed by accessing orbit overlap

errors. The latest gravity model yielded smaller orbit errors than the earlier model. This was to be expected since the MGS75D model used more MGS data in its creation than the MGS75B model. For the GCO phase of the MGS mission, orbit overlap errors were less than 0.2 m, 5 m, 30 m in the radial, transverse, and normal directions, respectively. For the mapping phase of the mission, the errors tended to be larger than the GCO phase. This was because the HGA was in the deployed configuration and was able to articulate. The orbit overlap errors during the Map-2 and Map-3 phases were determined to be less than 6 m, 100 m, 20 m in the radial, transverse, and normal directions, respectively. Obtaining higher resolution gravity models, which can only be obtained by reducing the MGS altitude, can further reduce these errors.

ACKNOWLEDGMENTS

MGS pictures and stats courtesy of the MGS and Mars web pages[16,17]. The work described in this paper was carried out at the Jet Propulsion Laboratory, California Institute of Technology, under contract with the National Aeronautics and Space Administration.

REFERENCES

1. Sjogren, W. L., D. N. Yuan, and A. S. Konopliv, Mars gravity field modeling with MGS, paper presented at Spring Meeting, AGU, Boston, MA, May 31 to June 4, 1999a.

2. Yuan, D. N., W. L. Sjogren, A. S. Konopliv, and A. B. Kucinskas, Gravity field of Mars: A 75th Degree and Order Model, J. Geophys. Res., in press 2001.

3. Moyer, T. D., Mathematical formulation of the Double-Precision Orbit Determination Program, *Technical Report 32-1527*, Jet Propulsion Laboratory, California Institute of Technology, Pasadena, CA, 1971.

4. Lawson, C. L., and R. J. Hanson, *Solving Least Squares Problem*, Society for Industrial and Applied Mathematics, Philadelphia, PA, 1995.

5. Bierman, G. J., *Factorization Methods for Discrete Sequential Estimation*, Academic Press, New York, 1977.

6. Folkner, W. M., J. A. Steppe, and S. H. Oliveau, Earth Orientation Parameter file description and usage, *Interoffice Memo. 335.1-11-93*, Jet Propulsion Laboratory, California Institute of Technology, Pasadena, CA, 1993.

7. Boucher C., Z. Altamimi, and L. Duhem, Results and analysis of the ITRF93, *IERS Tech. Note 18*, Obs. de Paris, 1994.

8. Folkner, W. M., DSN station locations and uncertainties, *Progress Rep. 42-128*, pp. 1-34 Jet Propulsion Laboratory, California Institute of Technology, Pasadena, CA, 1996.

9. Davies M. E., V. K. Abalakin, M. Bursa, J. H. Lieske, B. Morando, D. Morrison, P. K. Seidelmann, A. T. Sinclair, B. Yallop, and Y. S. Tjuflin, Report of the IAU/IAG/COSPAR Working Group on Cartographic Coordinates and Rotational Elements of the Planets and Satellites: 1994, *Celestial Mech. Dyn. Astron., 63,* 127-148, 1996.

10. Standish, E. M., and Newhall, X X, New accuracy levels for solar system ephemerides, in *IAU Symp. 172: Dynamics, Ephemerides and Astrometry of the Solar System*, edited by S. Ferraz-Mello et al., pp. 29-36, IAU, Paris, 1996.

11. Newhall, X X, J. G. Williams, and E. M. Standish, Planetary and Lunar Ephemerides, Lunar laser ranging, and Lunar physical librations, in *IAU Symp. 172: Dynamics, Ephemerides and Astrometry of the Solar System*, edited by S. Ferraz-Mello et al., pp. 37-44, IAU, Paris, 1996.

12. Jacobson, R. A., The orbital motion of the Martian satellites: An application of artificial satellite theory, *AAS Pap. 96-140*, AAS/AIAA Space Flight Mech. Meet., Austin, TX, 1996.

13. Jagjit M., S/C HGA phase center and line of boresight movements after deployment with azimuth and elevation gimbal positions, *Interoffice Memo. MSOP-98-011*, Lockheed Martin, Denver, Colo., Feb. 1998.

14. Semenov, B., private communication, 1999.

15. Yuan, D. N., The determination and error assessment of the Earth's gravity field model, Ph.D. thesis, University of Texas at Austin, 1991.

16. Web site for the Mars Global Surveyor, http://mars.jpl.nasa.gov/mgs/

17. Web site for the Mars Exploration Homepage, http://mars.jpl.nasa.gov/

Table 1. Mars Global Surveyor Mission Phases

MGS Mission Phase	From	To
AB-1	Nov. 7, 1997	Mar. 28, 1998
SPO-1	Mar. 28, 1998	Apr. 28, 1998
Solar Conjunction Period	Apr. 28, 1998	Jun. 4, 1998
SPO-2	June. 4, 1998	Sep. 23, 1998
AB-2	Sep. 23, 1998	Feb. 4, 1999
GCO	Feb. 4, 1999	Mar. 29, 1999
Map-1	Mar. 29, 1999	Aug. 4, 1999
Map-2	Aug. 4, 1999	Dec. 2, 1999
Map-3	Dec. 2, 1999	Apr. 18, 2000

Figure 1. The Mars Global Surveyor Orbit Viewed from the Sun

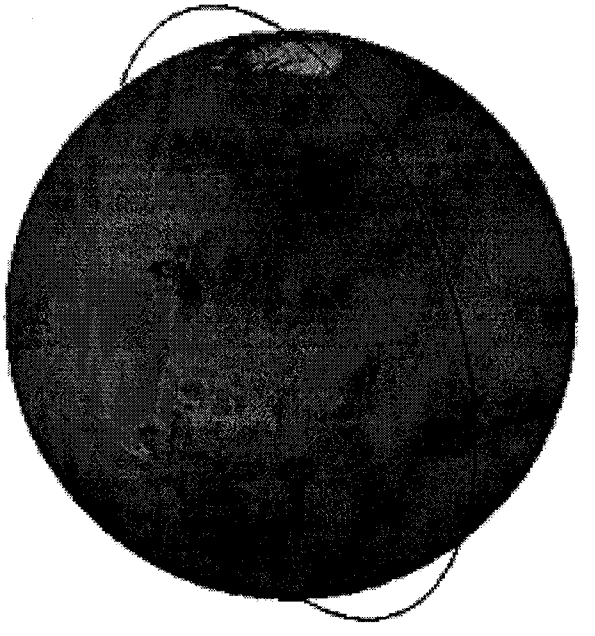

Figure 2. The Mars Global Surveyor spacecraft

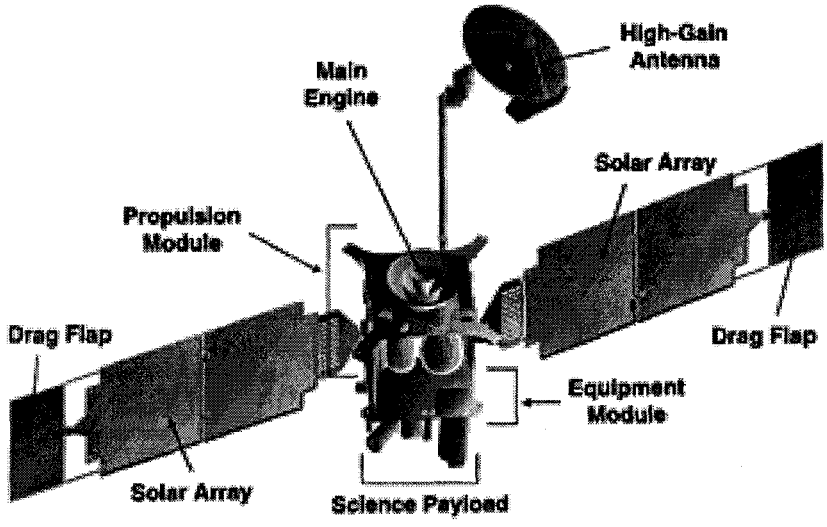

Figure 3: GCO Phase RMS Orbit Errors (Radial)

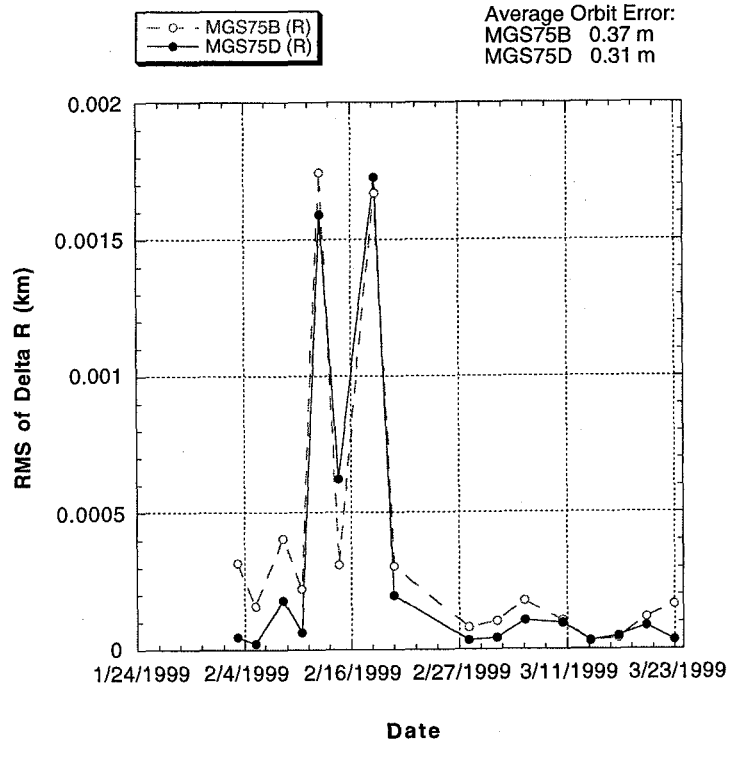

Figure 4: GCO Phase RMS Orbit Errors (Transverse)

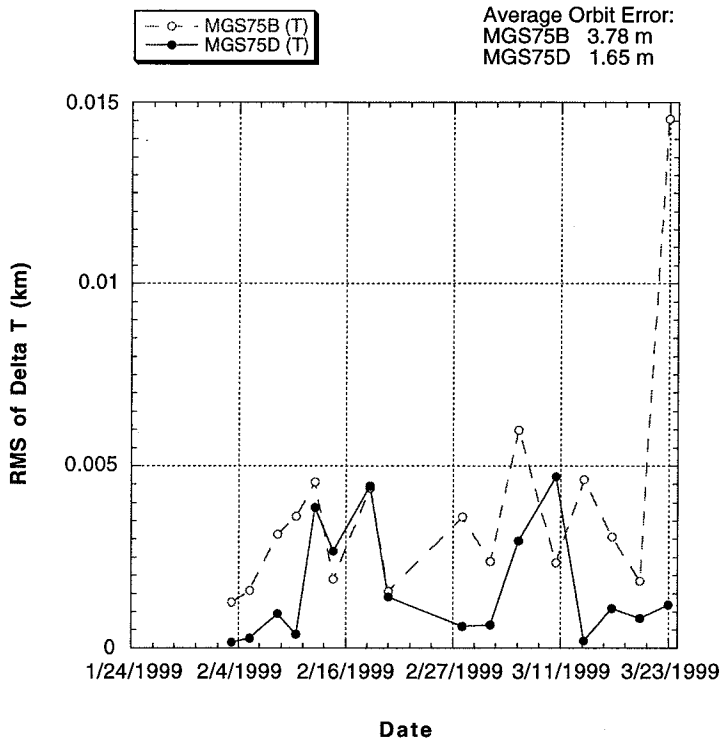

Figure 5: GCO Phase RMS Orbit Errors (Normal)

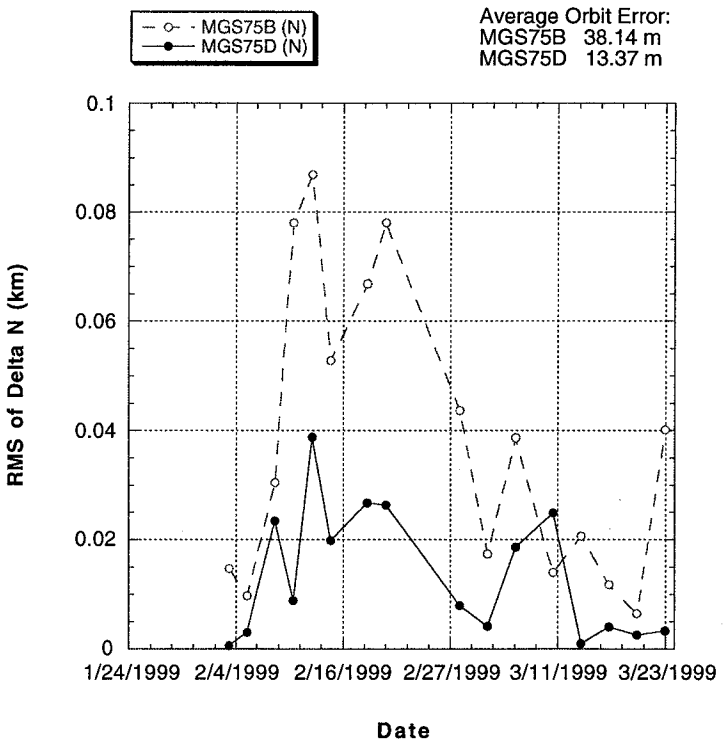

Figure 6: Mapping Phase RMS Orbit Errors (Radial)

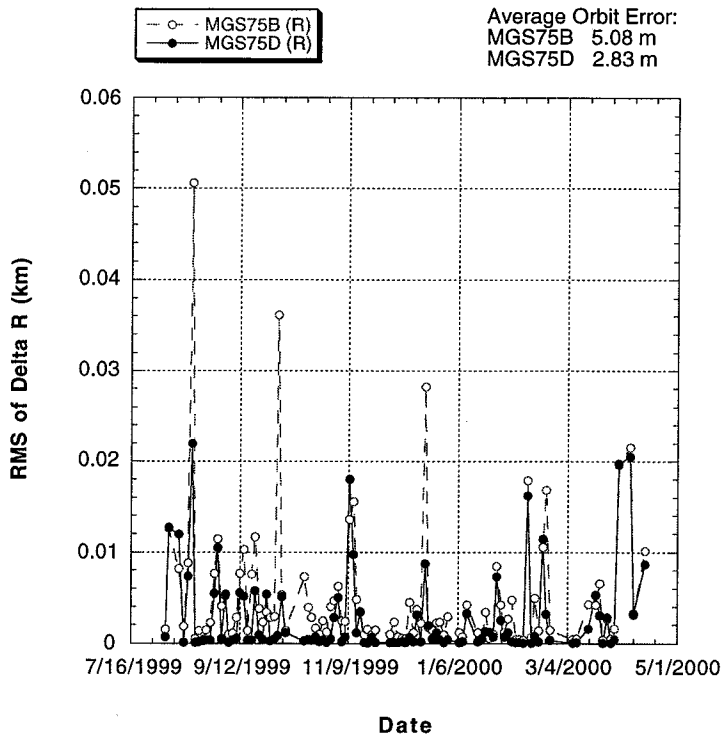

Figure 7: Mapping Phase RMS Orbit Errors (Transverse)

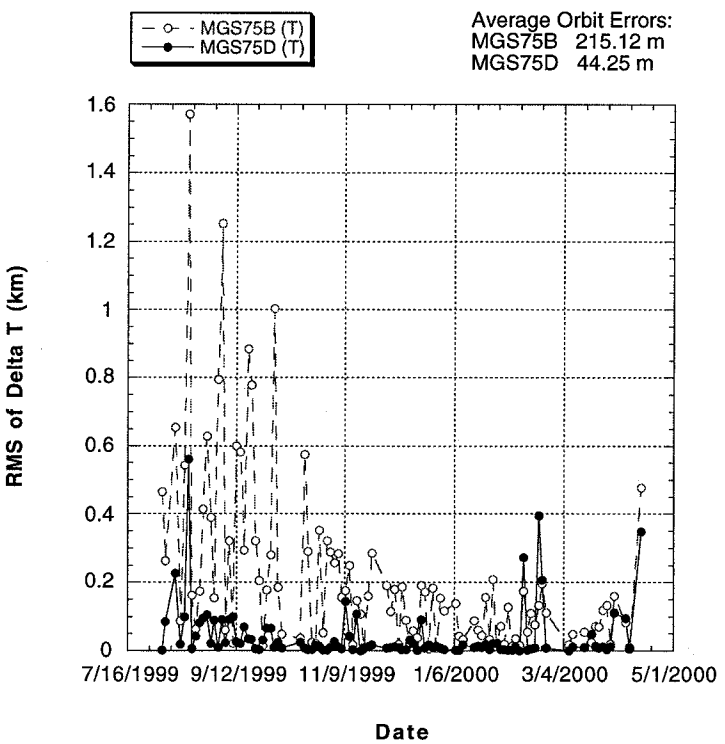

Figure 8: Mapping Phase RMS Orbit Errors (Normal)

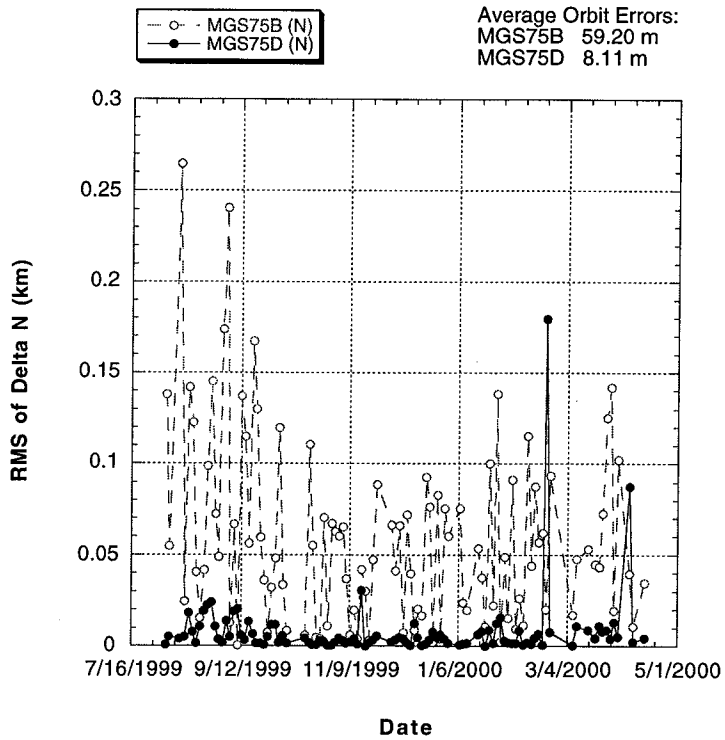

Figure 9: Doppler Residual Sample (units in mm/s)

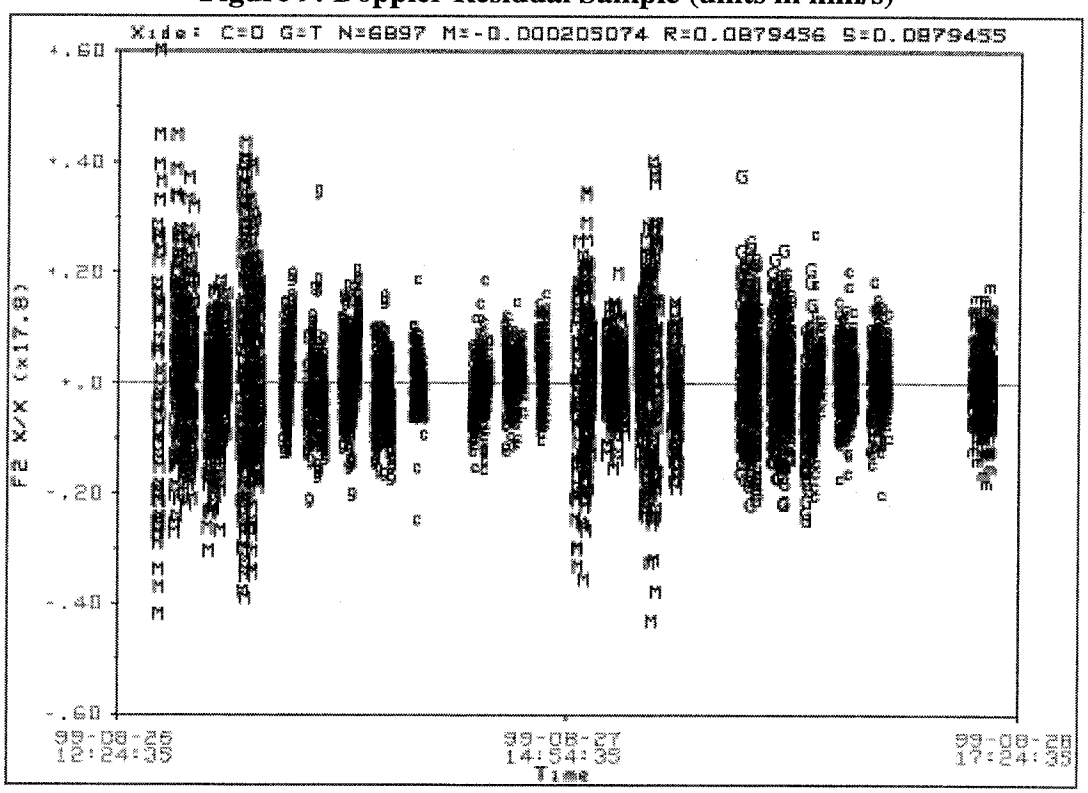

Figure 10: Range Residual Sample (units in m)

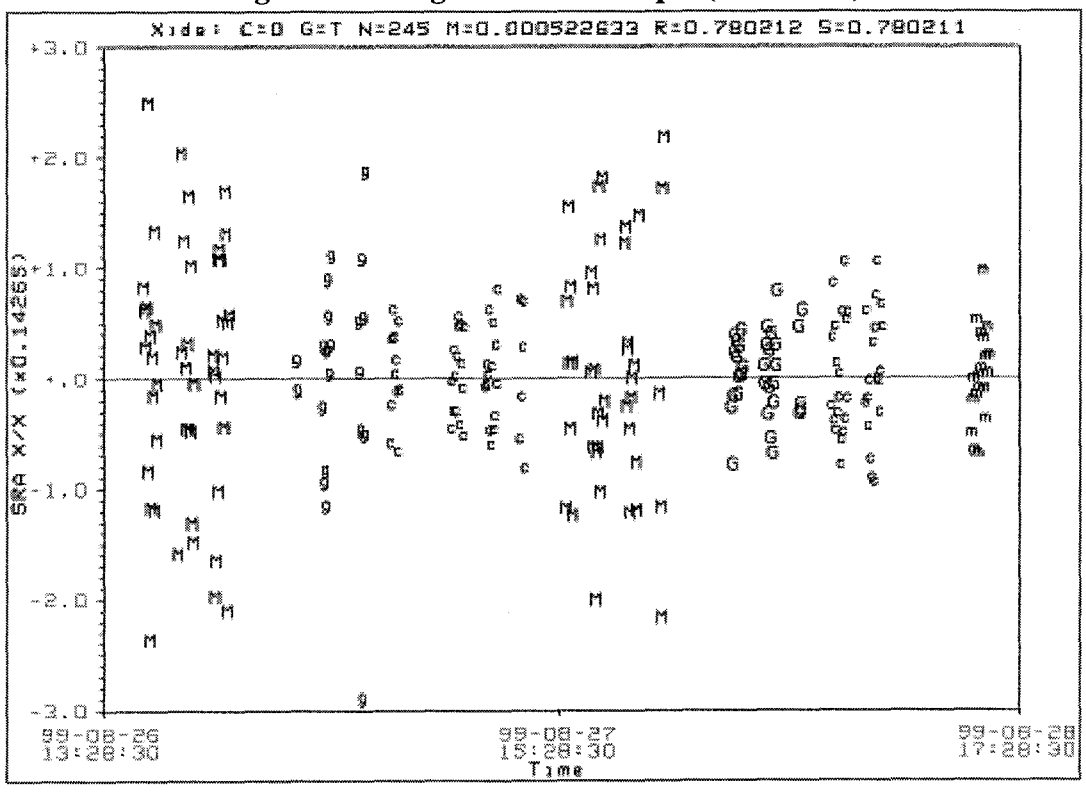

Figure 11: RMSof Two-way Doppler Residuals for Map2-3